

Pulsar timing in the Galactic Center

R. Della Monica^{1,*} and I. De Martino^{1,2,†}

¹*Departamento de Física Fundamental, Universidad de Salamanca, Plaza de la Merced, s/n, E-37008 Salamanca, Spain*

²*Instituto Universitario de Física Fundamental y Matemáticas (IUFFyM),
Universidad de Salamanca, Plaza de la Merced, s/n, E-37008 Salamanca, Spain*

We propose a novel approach which implements the relativistic calculations of the photon travel time into a robust timing model for pulsars orbiting supermassive black holes. We demonstrate the inability of current timing codes based on the post-Newtonian expansion of General Relativity to correctly estimate the relativistic time of arrival of the emitted pulses at an Earth-based observatory. We also show how a misestimation of the pulsar parameters can lead to the appearance of phase-dependent residual, which hints at a tremendous constraining power of the binary and intrinsic parameters for timing observations of potential pulsars at the Galactic Center.

I. INTRODUCTION

The next significant advancement in experimental gravitation is expected with the discovery of pulsars orbiting a supermassive black hole (SMBH). Pulsars, whose intrinsic rotational period variation is of the order of one part in 10^{15} per pulse period [1], are a remarkable tool for probing gravitational fields [2–4]. Pulsars in stellar binary systems allowed the detection of various general relativistic effects, including the decay of orbital periods due to the emission of dipolar gravitational waves [5–7]. However, these systems probe a relatively weak gravitational field with compactness $GM/Rc^2 \sim 10^{-5} \div 10^{-7}$ [8]. Here R represents the binary separation, and the component masses are of the order of solar masses. In contrast, a pulsar closely orbiting (*i.e.* with orbital periods ranging from 1 to 100 years) a SMBH, such as Sagittarius A* (Sgr A*) at the Galactic Center, would explore an entirely different gravity regime where the source mass of the gravitational potential well is of order of $\sim 10^6 M_{\odot}$.

The significance of pulsars in the Galactic Center is highlighted by the increasing number of radio pulsar searches within the central few parsecs of the Milky Way [9–13]. However, despite observational efforts, only five pulsars were discovered within 15 arcminutes of Sgr A* [10, 11], along with a single radio magnetar positioned 2.4 arcseconds away from Sgr A* (equivalent to 0.1 pc in projection) [14–16], and a millisecond pulsar within 1° from the Galactic Center [17]. This apparent failure to detect pulsars at the Galactic Center is attributed to interstellar scattering processes. In fact, photons travel through the turbulent and ionized interstellar medium located between the source and the observer, which broadens the pulses [18]. Such a temporal broadening strongly depends on the observing frequency ($\propto \nu^{-4}$) decreasing the effectiveness of the periodicity search techniques even for long-period pulsars. Additionally, temporal broadening cannot be corrected instrumentally [19]. Therefore, a potential solution would be to look at higher frequencies,

but the characteristic power-law spectra of pulsars ($\propto \nu^{\alpha}$ with $\alpha < 0$ [20]) implies that higher frequencies correspond to a lower intrinsic flux. For such a reason, high-frequency pulsar searches in the Galactic Center have not reported the detection of new pulsars even using Event Horizon Telescope (EHT) 2107 data [21, 22]. Nevertheless, the abundant population of young and massive stars orbiting Sgr A* suggests the potential presence of pulsars originating from Supernovae explosions in this population's massive end [23] and, depending on the specific population model, there would be between 100 and 1000 pulsars within the central parsec of the Galactic Center, with orbital periods < 100 years (including around 100 pulsars with orbital periods < 10 years) and over 10,000-millisecond pulsars [24–27]. Therefore, detecting at least one pulsar orbiting Sgr A* has become a scientific goal for forthcoming observational facilities, including the Square Kilometre Array¹ (SKA) [28], the Five-hundred-meter Aperture Spherical Telescope² (FAST) [29], the next-generation Very Large Array³ (ngVLA) [30], and the next generation Event Horizon Telescope⁴ (ngEHT) [31].

On the theoretical side, the analysis of Times Of Arrival (TOAs) of pulses emitted by pulsars, usually known as pulsar timing analysis, might potentially improve all previous tests of General Relativity in the strong field regime [32, 33]. For instance, pulsar timing analyses in the Galactic Center will enhance the mass determination precision of Sgr A*, and could provide measurements of the spin magnitude and orientation of the SMBH [8, 33] with a relative precision on the order of $10^{-4} \div 10^{-3}$. Furthermore, these analyses could yield measurements of the SMBH quadrupole moment [32–34], allowing a direct test of the no-hair theorem at the Galactic Center [35, 36]. In [37] a methodology for the numerical computation of fully relativistic propagation times for photons emitted in a generic spherically symmetric spacetime was introduced.

* rdellamonica@usal.es

† ivan.demartino@usal.es

¹ <https://www.skao.int/en>

² <http://fast.bao.ac.cn>

³ <https://public.nrao.edu/ngvla/>

⁴ <https://www.ngeht.org>

This can be applied to estimate the observational impact on the timing residuals of a change in the fundamental nature of the central object or in the underlying theory of gravity. In perspective, this study qualitatively suggests that the possible constraints that future pulsar observations at the Galactic Center would enable, on the extra parameters encoding deviations from the general relativistic scenario, can surpass by orders of magnitude the constraints arising from other probes in the Galactic Center [38]. This further demonstrates the paramount importance of pulsars orbiting SMBH as strong-field probes of gravity and motivates scientific and technical efforts required to successfully discover and time these kinds of objects. Forthcoming telescopes will benefit from a substantial increase in the collection areas and, among them, SKA has been demonstrated that may potentially achieve an accuracy on the pulse TOA measurement of the order of $\sigma_{\text{TOA}} \simeq 100\mu\text{s}$ for normal pulsars [39], *i.e.* with the binary companion being either a white dwarf, a neutron star, or another pulsar as well) at frequencies above 15 GHz [33] though all possible limiting effects on the precision of TOA measurements of young pulsars in the Galactic Center environment were considered (*i.e.* the signal-to-noise ratio of the measured pulses, the intrinsic pulse phase jitter and the changes in pulse shape caused by interstellar scintillation).

We aim to introduce a different approach for studying the TOAs of pulsars orbiting the SMBH in the Galactic Center which is based on a new methodology to compute the photon propagation time in black hole spacetimes previously introduced and tested in [37]. First, we will assume that pulsars at the Galactic Center actually exist and will be successfully detected and timed within the accuracy goal of $100\mu\text{s}$ per TOA. With these *ansatz* in mind, we will first summarize in Section II the theoretical framework in which we will move. Then, in Section III we will explain how, given a set of pulsar parameters, we can estimate the corresponding TOAs received by a distant observer using both the standard pulsar timing techniques based on post-Newtonian approximations and using our novel methodology. Here we will clearly show the failure of post-Newtonian formulas to correctly reproduce the relativistic results. Finally, we discuss our results and draw our conclusions in Section V.

II. THEORETICAL FRAMEWORK

In General Relativity, whenever one wants to describe the exterior gravitational field of static and spherically symmetric bodies, one has to search for spherically symmetric solutions to Einstein's field equations in vacuum. Looking for spherically symmetric solutions implies that one is looking for a metric tensor $g_{\mu\nu}$ whose components must satisfy certain symmetries, thus reducing the degree of freedom of the metric tensor and, hence, the number of free functions to solve for. In particular, the spacetime must be *stationary* and *static* and the metric

tensor reduces to $g_{\mu\nu} = g_{tt}dt^2 + g_{ij}dx^i dx^j$. Therefore, a convenient system of coordinates to employ is given by (t, r_s, θ, ϕ) , usually called the *spherical* (or *Schwarzschild*) *coordinate system* where the components of the metric tensor depend on (θ, ϕ) only through the solid angle which, in turn, implies that all off-diagonal terms in g_{ij} must be zero. This also gives that $g_{\theta\theta} = r_s^2$ and $g_{\phi\phi} = r_s^2 \sin^2 \theta$. Finally, there are only two unknown functions of the aerial radius to be determined (corresponding to the g_{tt} and g_{rr} components) and the metric tensor may be recast as

$$g_{\mu\nu} = \begin{pmatrix} A(r_s) & 0 & 0 & 0 \\ 0 & B(r_s) & 0 & 0 \\ 0 & 0 & r_s^2 & 0 \\ 0 & 0 & 0 & r_s^2 \sin^2 \theta \end{pmatrix} \quad (1)$$

which corresponds to the following metric elements

$$ds^2 = -A(r_s)dt^2 + B(r_s)dr_s^2 + r_s^2 d\Omega^2. \quad (2)$$

Here $d\Omega^2 = d\theta^2 + \sin^2 \theta d\phi^2$, and the unknown functions are $A(r_s)$ and $B(r_s)$. Let us remark that the line element in Eq. (2) only descends from symmetries imposed to a generic spacetime metric, without accounting for the field equations of General Relativity. For this reason, this line element is rather generic and can be used for any metric theory of gravity based on differential geometry [37]. In General Relativity, the solution of Einstein's field equations in vacuum returns the well-known Schwarzschild solution (here and in the rest of the paper we assume $G = c = 1$)

$$A(r_s) = B^{-1}(r_s) = 1 - \frac{2M}{r_s} \quad (3)$$

which is unique, obeys Birkhoff's theorem, and has only one free parameter, M , which corresponds to the mass of the central body. The post-Newtonian approximation of the spherically symmetric spacetime of General Relativity can be directly derived from the Schwarzschild solution in the weak-field, slow-motion limit, at any given order. The usual procedure to do this, however, is conventionally performed in a different system of coordinates, namely, the *harmonic coordinates*. To facilitate comparison between our results and those from the usual post-Newtonian approach to pulsar timing, we will adopt this system of coordinates, too. The Schwarzschild solution in Eq. (3) can be recast in harmonic coordinates by simply considering the coordinate transformation

$$r := r_s + M \quad (4)$$

which leads to

$$ds^2 = -\left(\frac{r-M}{r+M}\right) dt^2 + \left(\frac{r+M}{r-M}\right) dr^2 + (r+M)^2 d\Omega^2. \quad (5)$$

Since our main tool will be the geodesic motion in such spherically symmetric spacetime solutions, it is convenient to explicitly write down the geodesic equations for

the metric element in Eq. (2)

$$\ddot{t} = -\frac{2M\dot{r}\dot{t}}{r^2 - M^2} \quad (6)$$

$$\ddot{r} = \frac{M\dot{r}^2}{r^2 - M^2} - \frac{M\dot{t}^2(r - M)}{(r + M)^3} + (r - M)(\dot{\phi}^2 \sin^2 \theta + \dot{\theta}^2) \quad (7)$$

$$\ddot{\theta} = \frac{M\dot{\phi}^2 \sin(2\theta) + r\dot{\phi}^2 \sin(2\theta) - 4\dot{r}\dot{\theta}}{2(r + M)} \quad (8)$$

$$\ddot{\phi} = -\frac{2\dot{\phi}((r + M)\dot{\theta} \cot \theta + \dot{r})}{r + M} \quad (9)$$

where dots denote derivatives with respect to the affine parameter.

A. Light propagation in a spherically symmetric spacetime

For completeness, here we summarise the results we found in [37]. Relativistic corrections to the photon propagation are of paramount importance when dealing with pulsar timing. These corrections are taken into account when null geodesics are integrated. Nevertheless, to carry out the integration of the photon path, an appropriate initial condition search has been carried out to identify the right null trajectory connecting the emitter and observer at any epoch or, in other words, to solve the *emitter-observer* problem. In [37], a numerical methodology has been developed based on the generic asymptotically-flat spherically-symmetric spacetime in Eq. (2). Since one is considering a spherical symmetric spacetime, one can restrict to the equatorial plane $\theta = \pi/2$ though this may not coincide with the plane on which the orbit of the emitting object lies. The propagation of the photon on such a plane is then determined by the equation for the polar trajectory of the photon,

$$\frac{d\phi}{dr} = \frac{b}{r\sqrt{\Upsilon(r)}}, \quad (10)$$

and the differential equation for the coordinate time, t , as a function of the radial coordinate, r ,

$$\frac{dt}{dr} = \frac{r}{A(r)\sqrt{\Upsilon(r)}}, \quad (11)$$

where we have defined

$$\Upsilon(r) = \left(\frac{r^2 - b^2 A(r)}{A(r)B(r)} \right). \quad (12)$$

Here, we want to consider a pulsar at spatial coordinate $E(r_e, \phi_e)$ which emits a photon γ at coordinate time t_e , and an observer at spatial coordinate $O(r_o, \phi_o)$ detecting the photon at coordinate time t_o . Therefore, the equation (11) is solved to compute the travel time, $\Delta t = t_o - t_e$, while the equation (10) is used to solve for the impact

parameter b and, therefore, to solve the *emitter-observer* problem. This latter step is done by solving the following equation

$$\phi_o - \phi_e = \int_{r_e, \gamma}^{r_o} \frac{b}{r\sqrt{\Upsilon(r)}} dr. \quad (13)$$

Here, the integral in equation (13) depends on whether the photon path γ from E to O is direct or indirect, as illustrated in Figure 1.

Since we will consider only primary photons received by the observer⁵ only two possible scenarios are possible:

Direct propagation: the radial coordinate may increase monotonically going from r_e to r_o ;

Indirect propagation: the radial coordinate decreases up to a certain r_{\min} and then increases monotonically up to r_o .

In the first case, the integral in equation (13) can be recast as

$$\phi_o - \phi_e = \int_{r_e}^{r_o} \frac{b}{r\sqrt{\Upsilon(r)}} dr, \quad (14)$$

while, in the other case, it would read

$$\phi_o - \phi_e = \int_{r_e}^{r_{\min}} \frac{b}{r\sqrt{\Upsilon(r)}} dr + \int_{r_{\min}}^{r_o} \frac{b}{r\sqrt{\Upsilon(r)}} dr. \quad (15)$$

We solve numerically the emitter-observer problem and have access to the impact parameter b of the photon corresponding to the primary image of the source for the observer in O . We can now approach the problem of determining the travel time of the photon from E to O . Since the line element in equation (2) is asymptotically flat for a sufficiently far observer (as is the case for an Earth-based observer for a test particle orbiting Sgr A*), we can assume that the observer measures the coordinate time t and thus the travel time is simply the integral of Eq. (11) over the photon's path γ :

$$\Delta t \equiv t_o - t_e = \int_{r_e, \gamma}^{r_o} \frac{r}{A(r)\sqrt{\Upsilon(r)}} dr. \quad (16)$$

In the case of the Earth, one must add the relativistic corrections due to the presence of the Sun's gravitational field and the motion of Earth around it. Still, we can also safely assume a weak-field approximation for the Sun [40]. Finally, considering the solution of the integral between two generic radial coordinates,

$$T(r_1, r_2) = \int_{r_1}^{r_2} \frac{r}{A(r)\sqrt{\Upsilon(r)}} dr, \quad (17)$$

⁵ We will not consider photons whose path bend so strongly that they reach the observer after one or more complete turns around the central object

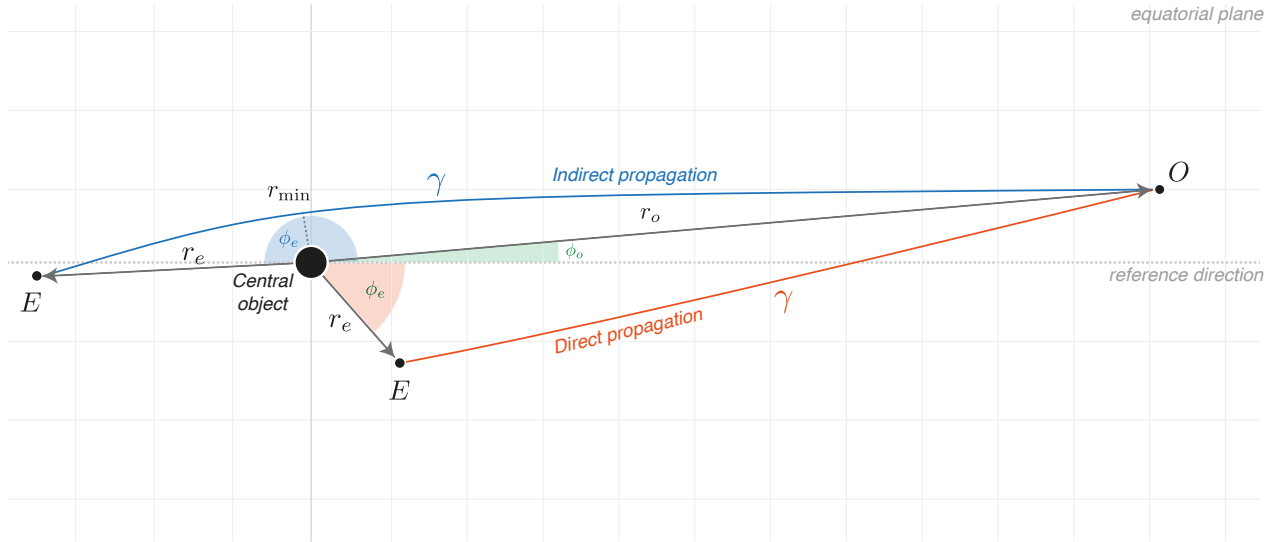


Figure 1. Illustration of the configuration for the emitter-observer problem. The emitter is located at a point E that is identified by polar coordinates (r_e, ϕ_e) , while the observer receiving the photon is located at point O with coordinates (r_o, ϕ_o) . Considering only primary photons received by the observer (*i.e.* we do not consider photons that graze so close to the unstable photon orbit of the central object that their paths bend so strongly, $\Delta\phi > 2\pi$, that they reach the observer after one or more complete turns around the central object) only two possible scenarios are possible: (*green path*) the radial coordinate increases monotonically going from r_e to r_o propagating directly ($r_e \rightarrow r_o$) from the emitter to the observer; (*purple path*) the photon leaves the observer with a decreasing radial coordinate (*i.e.* a negative radial velocity) then reaches a minimum distance r_{\min} from the central object after which it starts increasing again up to the observer position. We call the latter configuration *indirect propagation* ($r_e \rightarrow r_{\min} \rightarrow r_o$).

we can express the direct and indirect propagation by

$$\Delta t_{\text{direct}} = T(r_e, r_o), \quad (18)$$

$$\Delta t_{\text{indirect}} = T(r_e, r_{\min}) + T(r_{\min}, r_o). \quad (19)$$

As for the case of the emitter-observer problem, while an analytic solution in terms of Jacobi elliptic function exists for the case of the Schwarzschild spacetime, in the most general case one has to approach the problem numerically.

In [41], an analytical closed-form solution, for a non-inclined circular orbit, has been found for a Schwarzschild spacetime in terms of Jacobi elliptic function. To show the effectiveness of our approach, we particularized the calculation of the time delay for the Schwarzschild spacetime and compared the numerical results with the exact solution given by [41]

$$\Delta t_{\text{ex}} = \frac{GM}{c^3} (T_{\text{ex}}(r_o; b) \pm T_{\text{ex}}(r_e; b)). \quad (20)$$

Here, the sign \pm depends on whether the integration path is direct or indirect and the functions $T_{\text{ex}}(r; b)$ are, for a specific impact parameter, given by

$$T_{\text{ex}}(r; b) = \frac{2}{\sqrt{r_4(r_3 - r_1)}} (T_1 + T_2 + T_3 + T_4) + T_\infty, \quad (21)$$

where we have defined the terms

$$T_1 = \left(\frac{r_3^3}{r - 2} + \frac{1}{2}(r_4 - r_3)(r_3 - r_1 + 4) \right) F(x, k), \quad (22)$$

$$T_2 = -\frac{1}{2}r_4(r_3 - r_1)E(x, k), \quad (23)$$

$$T_3 = -2(r_4 - r_3)\Pi\left(x, \frac{k^2}{c_1}, k\right), \quad (24)$$

$$T_4 = -\frac{8(r_4 - r_3)}{(r_4 - 2)(r_3 - 2)}\Pi(x, c_2, k), \quad (25)$$

and T_∞ encodes all the diverging (for $r \rightarrow \infty$) terms as follows

$$T_\infty = \frac{b\sqrt{R(r)}}{r - r_3} + 2 \ln \left(\frac{\sqrt{r(r - r_1)} + \sqrt{(r - r_4)(r - r_3)}}{\sqrt{r(r - r_1)} - \sqrt{(r - r_4)(r - r_3)}} \right). \quad (26)$$

In the previous relations, all quantities that appear are expressed in geometrized units, the functions F , E and Π are Jacobian elliptic integrals [42], r_1 , r_2 , r_3 , r_4 are the roots of the function $R(r)$ which is derived from the function $\Upsilon(r)$ in Eq. (12), upon factorization of the dependence on the impact parameter b , x is an auxiliary variable and k , c_1 and c_2 are all constant terms built from the roots r_1 , r_2 , r_3 , r_4 .

In Figure 2 we show (*i*) the perfect agreement (within the adopted numerical tolerance of 10^{-6} s) between our numerical prediction and the analytical result for the

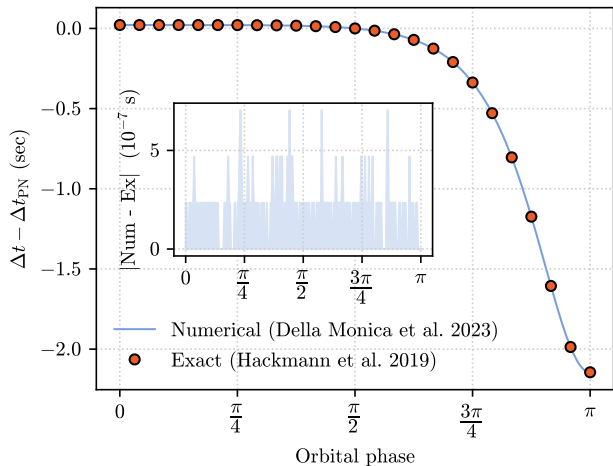


Figure 2. Residuals (in seconds) between the post-Newtonian approximation and the fully relativistic delay (for both the exact formula as presented in [41], *orange dots*, and our numerical methodology (blue solid line)) as a function of the orbital phase for a toy model circular orbit with $r = 100M$ and an inclination of $i = 60^\circ$. The 1PN formula in Eq. (27) fails in reproducing the correct results for the photon propagation time, with residuals that can reach ~ 2 s at superior conjunctions, when the photon has to travel longer in the black hole gravitational field to reach the distant observer. The inset reports the residuals between the analytical estimation and the numerical one.

Schwarzschild spacetime for a non-inclined circular orbit of radius $100M$ and an observer at a distance of 10^9M , which validate our approach and pipelines; and *(ii)* the differences with respect to the usual post-Newtonian approximations. Let us remember that, at 1PN order, the photon travel time from the emitter’s position to the observer’s position can be recast as [40, 43]

$$\Delta t_{\text{PN}} = \Delta t_{\text{R}} + \Delta t_{\text{Sh}} + \Delta t_{\text{geo}}. \quad (27)$$

Here, Δt_{R} is the Rømer delay related to the photon propagation time across the emitting pulsar’s orbit

$$\Delta t_{\text{R}} = \frac{|\vec{r}_{\text{o}} - \vec{r}_{\text{e}}|}{c}, \quad (28)$$

and Δt_{Sh} is the Shapiro time delay related to the time dilation of photons grazing the central object and is given by [4, 41]:

$$\Delta t_{\text{Sh}} = -\frac{2GM}{c^3} \ln \left(\frac{2|\vec{r}_{\text{o}}|}{|\vec{r}_{\text{e}}| + \vec{r}_{\text{e}} \cdot \hat{k}} \right). \quad (29)$$

It is worth noticing that both the Rømer and the Shapiro delay are computed by assuming that the photons propagate on a straight line. The last term, dubbed geometrical time delay, takes into account the curved photon path and is given by [4, 44]

$$\Delta t_{\text{geo}} = \frac{2GM}{c^3} \left(\frac{|\vec{r}_{\pm} - \vec{r}_{\text{s}}|}{R_E} \right)^2. \quad (30)$$

Model	a (AU)	a (mas)	e	T	Γ (10^{-4})
Toy 0	1025	125	0.88	16 yr	3
Toy 1	175.4	21.1	0.800	1.162 yr	11
Toy 2	43.8	5.28	0.800	52.9 days	45
Toy 3	5	0.60	0.786	2.0 days	374

Table I. The orbital parameters (semi-major axis in both physical units and angular dimension assuming a distance of $D = 8$ kpc for the Galactic Center, eccentricity and orbital period) of the toy models used for our analysis. The four orbits considered scan an increasingly strong gravitational regime, as quantified by the relativistic parameter $\Gamma \equiv r_g/r_p = GM/ac^2(1 - e)$, corresponding to the ratio of the gravitational radius of the central object and the orbital separation of the pulsar at pericenter.

where we have defined the gravitational-lensing Einstein radius

$$R_E = \left(\frac{4GM}{c^2} (\vec{r}_{\text{o}} - \vec{r}_{\text{e}}) \cdot \hat{k} \right) \quad (31)$$

and the vector $\vec{r}_{\text{s}} = \vec{r}_{\text{e}} - (\vec{r}_{\text{e}} \cdot \hat{k})\hat{k}$ is the sky-plane projection of the emitter position (*i.e.* the apparent position that the pulsar would have in the observer reference frame without light bending), while

$$\vec{r}_{\pm} = \frac{\vec{r}}{2} \left(1 \pm \sqrt{1 + \frac{4R_E^2}{|\vec{r}_{\text{s}}|^2}} \right), \quad (32)$$

is the sky-plane lensed position seen by the distant observer.

Since the timing delay equation (20) captures strong field effects, it provides a better description of the photon propagation time with respect to the 1PN approximations in equation (27) when applied to a pulsar-SMBH system. The two approaches differ an amount of the order of seconds when considering a circular orbit with a radius of about a hundred gravitational radii, as shown in Figure 2.

It is clear from Eq. (20) that the specific expression derived in [41] is only valid under the assumption of a Schwarzschild spacetime geometry and for a pulsar on a circular orbit with zero inclination. For a more general orbital model, or for different black hole geometries (even if spherical symmetry is preserved) such an expression should be modified accordingly and might even result in the impossibility of solving the corresponding integrals analytically. On the other hand, the approach developed in [37] and summarised in this section is more general and allows the computation of the propagation times of photons for any spherically symmetric spacetime and any emitter-observer configuration capturing all relativistic effects.

III. PULSAR TIMING TECHNIQUES AND PIPELINES

Using pulsar timing techniques, one can measure the TOAs of pulses emitted by a pulsar far away from the observer, monitor them on a timescale of years, and fit these TOAs to a model, namely a timing model. The latter is then used to link the measured TOA and the time of emission at the pulsar, allowing the computation of the pulse phase of emission accounting for the inherent variations in its period. In such a way, for pulsars in binary systems, one obtains a very precise estimation of the pulsar intrinsic parameters, *e.g.* intrinsic period and spin-down rate, and of the orbital parameters, *e.g.* masses and orbital period.

Low-mass-ratio pulsar binary systems do not belong to a strong relativistic regime. Therefore, the evolution of such systems can be studied through a post-Newtonian treatment of both the orbital motion and photon propagation, which returns a timing model whose precision is below the experimental uncertainty on the TOAs. For this reason, all the pulsar timing codes available nowadays adopt this approach. Conversely, high-mass ratio binary pulsars are in a strong field gravitational, and 1PN approximation of both the orbital motion and the photon propagation time cannot provide a timing model that accurately reproduces the TOAs (as shown, for instance, in Figure 2). As a consequence, residuals of the timing models are not adequately calculated undermining the fitting capabilities of usual timing codes. We propose a novel approach which implements the relativistic calculations of the photon travel time into a more robust timing model for pulsars orbiting SMBHs. We will perform a proof-of-concept analysis to investigate the failure of weak field approximation and the advantages of our methodology in the framework of parameter estimation for pulsars at the Galactic Center with SKA.

A. Pulsar timing in the weak-field: current techniques and pipelines

Most of the known pulsar binary systems are characterised by a low mass ratio. For this reason, all the pulsar timing codes available nowadays adopt PN approximation to compute the timing model.

The underlying mathematical framework and the accuracy in reproducing the TOAs are at the core of any code which aims to provide a timing model. Nevertheless, the rising sensitivity of radio observational facilities and the increasing diversity of pulsar populations discovered required improvements in the timing models accordingly. For many years, a very popular choice for pulsar timing was TEMPO⁶, which provides 100 ns of timing accuracy for

normal binary pulsar systems. Remarkably, it helped in numerous significant discoveries, such as the indirect detection of gravitational wave emission and other relativistic effects in pulsar binaries [45, 46], the first detection of extrasolar planetary systems [47], and the discovery of millisecond and submillisecond pulsars [48, 49]. However, an updated version of TEMPO, namely TEMPO2 [43, 50], was developed to reach the higher accuracy demanded by Pulsar Timing Array collaborations [51–54] to achieve the direct detection of the gravitational radiation emitted by pulsar systems. TEMPO2 is capable of reaching ~ 1 ns of timing accuracy for normal binary pulsar systems thanks to an improved characterization, with respect to TEMPO, of all the systematic effects that contribute to the resulting TOA, including tropospheric delays, pulse dispersion and updated estimates of secular orbital effects and Einstein and Shapiro delays. Recently, PINT [55] based on the same theoretical principles of TEMPO and TEMPO2, was proposed to offer a modern coding environment that allows also for cross-checking the results obtained across the different implementations.

The whole procedure, which finally returns the physical parameters of the system and the estimation of the relativistic effects, is schematically depicted in Figure 3. The first step is, of course, to measure the TOAs of pulses from a specific pulsar at a radio observatory. Such a measurement is done over an extended period (we will call N_{data} the number of recorded TOAs for a specific pulsar), and must ensure that the observed TOAs accurately reflect arrival times in an inertial reference frame. Each measured arrival time must be transformed into the reference frame of the pulsar constructing the timing model. Then, if the residuals between the reconstructed pulses and the measured TOAs are not negligible and do not show a random structure, then the model is poorly determined and the estimation of the parameter is not robust. Such discrepancies would arise for unaccounted-for binary companions or parameters, irregularities in the pulsar’s spin-down, or inaccurate estimation of astrometric or rotational parameters, among other effects⁷.

In general, the timing model for a non-relativistic binary pulsar system is given by

$$\tau_i = \text{TOA}_i - \Delta_{\odot} - \Delta_{\text{IS}} - \Delta_{\text{B}}, \quad (33)$$

where TOA_i is the time of arrival at the observatory of the i -th pulse, τ_i is the proper time in the pulsar’s inertial reference frame, Δ_{\odot} corresponds to the conversion to the Solar System barycenter frame, Δ_{IS} incorporates the transformation to the binary barycenter frame, and Δ_{B} accounts for the conversion to the pulsar frame. More specifically, Δ_{\odot} links the observed TOAs to the arrival

⁶ <https://tempo.sourceforge.net>

⁷ The full set of intrinsic, astrometric and binary parameters from which the timing model depends comprises more than 60 entries (albeit not all independent of each other) and is reported in Table A.1 of [43].

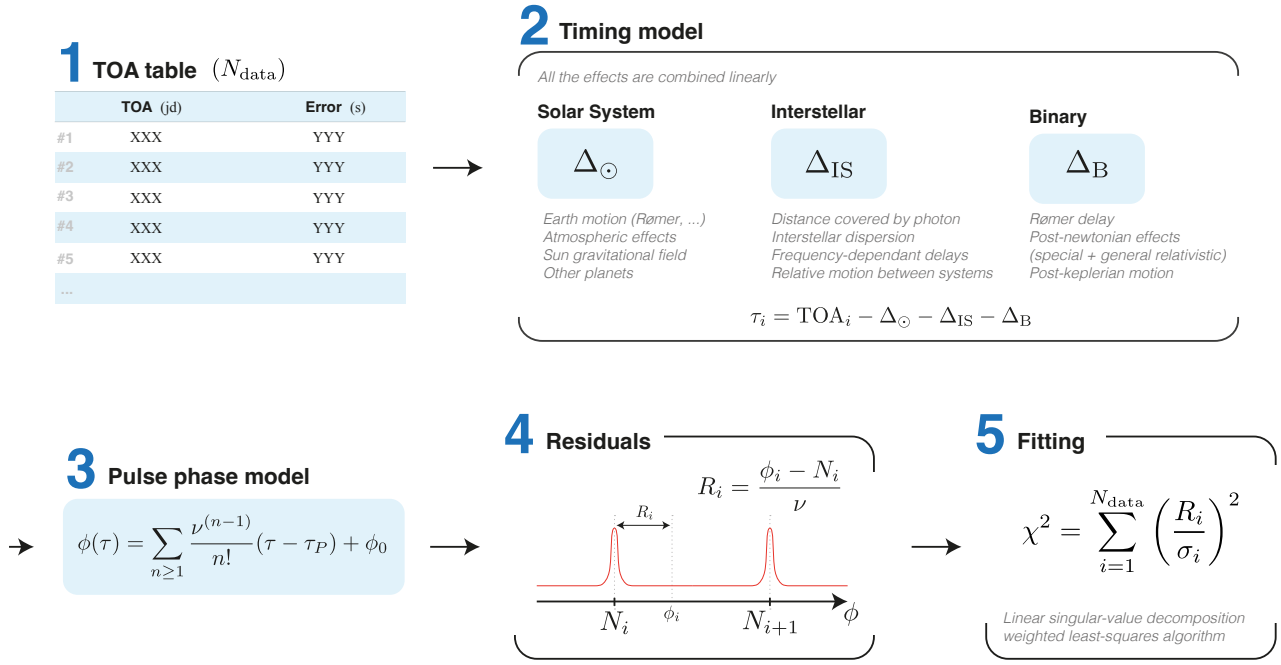


Figure 3. A schematic representation of the timing technique used in popular tools like **TEMPO2**. Observed TOAs are converted into barycentric proper emission times in the pulsar’s reference frame, τ , using a timing model that accounts for various classical and relativistic delays. These emission times are then linked to the emitted pulse sequence by modeling the pulse phase as a Taylor series, incorporating the pulse period (or frequency), its temporal variation, and potentially higher derivatives. The timing residual, R_i , is the difference between the calculated pulse phase and the nearest integer N_i , expressed in time units by dividing by the frequency or multiplying by the period. A χ^2 statistic is used to evaluate the alignment of the timing model with the observed TOAs. The best-fit timing model is determined by the parameters that minimize residuals and eliminate significant phase-dependent systematics.

time in the barycentric coordinate time at the Solar System barycenter, and accounts for vacuum propagation delays due to the Earth’s orbital motion, its spin, the Earth’s precession and nutation (considering that the observatory is situated on Earth), and any other delays due to the signal’s passage through the Earth’s atmosphere and the Solar system. This component links the observed TOAs to the arrival time in the barycentric coordinate time at the Solar System barycenter. Δ_{IS} incorporates delays attributed to the system’s secular motion and due to the signal traversing the interstellar medium. Finally, Δ_{B} includes delays due to the binary orbital motion and the signal’s passage through the gravitational field of the companion. The term Δ_{B} contains the relativistic contribution to the total photon propagation time produced in the binary pulsar system as a linear sum of post-Newtonian delays: the geometric Rømer delay in equation (28), a pseudo-delay reflecting the aberration of the radio beam caused by binary motion, the Einstein delay that encompasses both gravitational redshift and special relativistic time dilation in the pulsar frame, and the Shapiro delay in equation (29) and is given by

$$\Delta_E = \gamma \sin u, \quad (34)$$

where γ is a theory dependent parameter (more details

are reported in [40, 43]) and u is the pulsar’s eccentric anomaly. When one considers an infinite mass ratio between the pulsar and the massive companion (as a pulsar around a SMBH), the term Δ_{B} reduces to the Δ_{PN} introduced in Eq. (27). Finally, the binary motion is obtained from a post-Keplerian binary orbit in General Relativity [32, 40, 46, 56–60].

Once the proper time is obtained by applying equation (33), one can compute the corresponding pulse phase. In particular, if the pulsar period P were perfectly constant (or, equivalently its angular frequency ν), all the reconstructed proper times should be equally spaced and one would get integer steps from an initial phase ϕ_0 . However, pulsars experience a rotational spin-down due to the magnetic-dipole braking [60]. Therefore, the pulsar period is not perfectly constant (for all practical purposes one can consider only the first derivative, namely $\dot{\nu} = -\frac{\dot{P}}{P^2}$) implying a modification of the relation between the pulse phase ϕ and the proper time of the pulses

$$\begin{aligned} \phi(\tau) &= \sum_{n \geq 1} \frac{\nu^{(n-1)}}{n!} (\tau - \tau_P) + \phi_0 \\ &\approx \phi_0 + \frac{\tau - \tau_P}{P} - \frac{\dot{P}}{2P^2} (\tau - \tau_P)^2, \end{aligned} \quad (35)$$

where a constant spin-down rate is considered. If one knew the true theoretical parameters used for the timing model, then the computed $\phi_i - \phi_0$ will be an integer number N_i corresponding to the position of the given pulse in the pulse sequence (with the pulse at ϕ_0 corresponding to the 1st received). Nevertheless, the true parameters are not known *a priori*, and data are affected by the measurement noise. Therefore, the deviations of these pulse phases from the nearest integer are finite, and are quantified by the timing residual of the i -th pulse as

$$R_i = \frac{\phi_i - N_i}{\nu} = (\phi_i - N_i)P \quad (36)$$

corresponding to the time since (or to) the nearest actual pulse emitted by the pulsar (see panel 4 in Figure 3). Thus, given a set of N_{data} recorded TOAs for a specific pulsar, one can quantify the agreement of the timing model to the observational data by computing the χ -squared

$$\chi^2 = \sum_{i=1}^{N_{\text{data}}} \left(\frac{R_i}{\sigma_i} \right)^2, \quad (37)$$

where the σ_i represent the observational uncertainties on the TOAs. Finally, one can apply the least-squares method iteratively to find the set of parameters that minimizes the χ -squared. If those best-fit parameters do not produce any phase-dependent systematic in the residuals, the latter will only include measurement noise, and the timing model will return a robust estimation of both the pulsar's parameters and the relativistic effects experienced by the photon.

B. Pulsar timing in strong-field regime

Pulsars in tight orbits around Sgr A*, as those listed in Table I, are in a strong-field regime. Therefore, the methodology outlined in the previous section will fail in reproducing the observed TOAs because the 1PN approximation cannot accurately capture the relativistic effects. Indeed, it heavily relies on two assumptions:

- (i) the gravitational regime has to be sufficiently weak to consider that all relativistic effects can be combined linearly to compute the overall propagation time as in equation (33) [43];
- (ii) the approximation made by truncating at 1 PN order the description of the motion of both the binary system and photons are below the accuracy goal (~ 1 ns) and, most importantly, are much smaller than the pulsar intrinsic period P .

The latter condition is needed to interpret the timing residuals correctly. If the timing model is not accurate then the i -th pulse within the whole pulse sequence cannot be correctly identified and the whole procedure loses

its predictive capability [43]. For instance, if one considers double-neutron-star binaries, these deviations are already large compared to the 1 ns accuracy goal [43]. Consequently, in more extreme cases, these deviations became huge. Indeed, in the mildly relativistic pulsar-SMBH binaries (like the Toy 0 in Table I) the deviations between the 1PN formulation of the photon propagation time and the geodesic approach can be as large as 2 s. Moreover, in such a system one cannot linearly separate the different effects and a fully geodesic description is required, which will require incorporating the techniques developed for solving the emitter-observer problem [37] and changing the way to generate a phase-connected estimation of the timing residuals. The whole process is schematically summarised in Figure 4, and it is composed of the following steps:

- (a) Once the orbit has been integrated numerically, we sample a given number (N_{dense}) of equally spaced (in terms of proper time τ) points $\{\tau_i\}_{i=1}^{N_{\text{dense}}}$. Those are a subset of the whole sequence of all pulses (N_{pulses}) emitted over the considered timespan. For instance, considering a pulsar with a pulse period $P = 2$ s and an orbital model like Toy 1 in Table I we would have $N_{\text{pulses}} = 1.84 \times 10^7$ pulses emitted over every orbital period.
- (b) For each of the sampled points, we solve the emitter-observer problem and obtain an estimate of the relativistic propagation time, $\Delta t_{\text{relativistic}}$ using equation (19).
- (c) In such a way, we can compute the time of arrival at the distant observer for all the photons emitted at proper times $\{\tau_i\}_{i=1}^{N_{\text{dense}}}$, and it is given by

$$\text{TOA}_i = t(\tau_i) + \Delta t_{\text{Relativistic},i}, \quad (38)$$

where $t(\tau_i)$ is the coordinate time of emission and it is computed directly from the 0-th geodesics equation. Moreover, the term $\Delta t_{\text{Relativistic},i}$ only takes into account the relativistic contribution to the photon travel time.

- (d) Next, we reconstruct the function $\text{TOA}(\tau)$ between the proper time of emission in the pulsar's reference frame and the TOAs in the reference frame of a distant observer. The function $\text{TOA}(\tau)$ contains contributions from both classic or relativistic delays, and it is monotonically increasing because the principle of causality in General Relativity is preserved. The 1PN approximation of this function is given in equation (33). Nevertheless, we reconstruct the function $\text{TOA}(\tau)$ at N_{dense} points numerically and we invert it by interpolation. We adopt a spline interpolator whose order of the interpolation must be self-consistent with the order of convergence of the Runge-Kutta algorithm used for the geodesic integration. Moreover, the number

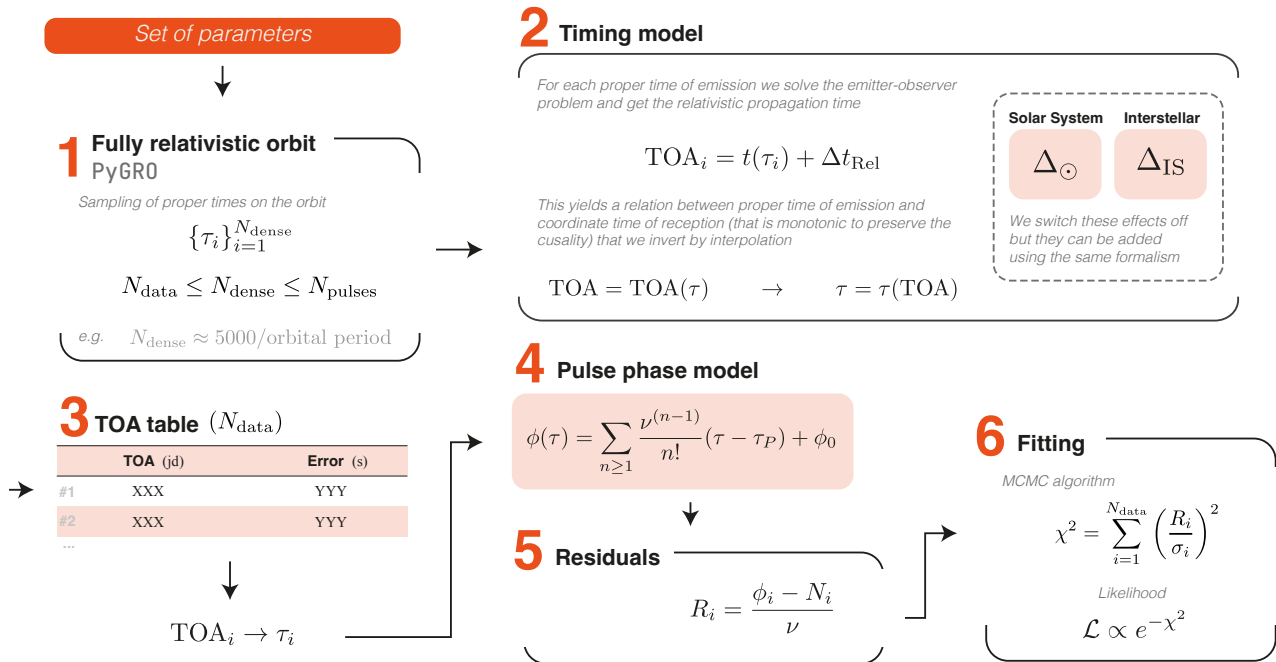


Figure 4. A schematic overview of the timing technique that we propose in this work. For a given set of intrinsic, astrometric, and orbital parameters of a pulsar orbiting a SMBH, we calculate a fully relativistic orbit by integrating the geodesic equation, Eqs. (6)-(9). The orbit is sampled at N_{dense} equally spaced points in proper time, $\{\tau_i\}_{i=1}^{N_{\text{dense}}}$. At each point, the emitter-observer problem is solved to estimate the relativistic propagation time for a distant observer. This establishes a map between the observed TOA and the proper emission time, which is inverted using spline interpolation. The resulting function, $\tau(\text{TOA})$, is applied to the observed TOAs to determine the barycentric proper emission time in the pulsar’s reference frame. Using standard timing techniques, we calculate the residuals, R_i , and the χ^2 statistic, which defines a likelihood function, \mathcal{L} , employed for Bayesian parameter estimation.

of points, N_{dense} , at which we sample the function $\text{TOA}(\tau)$ must fulfil the following condition

$$N_{\text{data}} \leq N_{\text{dense}} \leq N_{\text{pulses}}.$$

Here N_{data} represents the number of measurements in our TOA dataset, and N_{pulses} is the total number of pulses emitted by the pulsar over the considered timespan.

The most accurate reconstruction of the function $\text{TOA}(\tau)$ would be obtained if $N_{\text{dense}} = N_{\text{pulses}}$, *i.e.* a 1 : 1 correspondence between emitted pulses, integrated photon paths, and computed TOAs at the observer’s location. On the other hand, setting $N_{\text{dense}} = N_{\text{data}}$ would guarantee the fastest (in terms of computational time) option but would provide a robust reconstruction of the $\text{TOA}(\tau)$ function only if N_{dense} computed photon TOAs correspond exactly to the pulses, in the pulses sequence, that are measured at the observatory. However, this information is not known *a priori* and one cannot know to what position in the pulse sequence a given measured TOA corresponds. Therefore, we have found that N_{dense} roughly 50 times N_{data} provides a robust reconstruction of the photon travel time profile. We also check that increasing N_{dense} resulted in an improvement on

the interpolated $\text{TOA}(\tau)$ function that is below the instrumental sensitivity or the available measurement uncertainty. Finally, the contributions from the interstellar medium, (Δ_{IS}), the gravitational interaction of the photon with the Solar System gravitational field (Δ_{\odot}), the clock and atmospheric corrections included in TEMPO2 are not considered. However, since the gravitational field of the pulsar-SMBH binary system does not play a role in these terms, they belong to a weak field regime and can be added linearly *a posteriori* (as done in TEMPO2).

Using this timing model, we can translate TOAs in the observer reference frame into proper times in the pulsar reference frame. Then, we can proceed as with TEMPO2, we compute the pulse phase considering the first-order evolution of the pulse period in equation (35) and the residuals R_i for each pulse as given in equation (36).

IV. RESULTS

Let us now summarize the results of our analysis and the main differences with the 1PN approach.

A. Qualitative analysis of parameter estimation sensitivity

To appreciate how the shape and amplitude of the timing residuals change by over (under) estimating the orbital and intrinsic parameters of a pulsar, we perform a qualitative analysis of the TOA deviations. In Figure 5, we show the timing residuals over 9 orbital periods for the Toy 2 model listed in table I.

In the top line, we considered the effect of a misestimation of the intrinsic pulsar period P and its derivative \dot{P} and show that both drastically alter the time of arrivals by linearly and quadratically drifting the residuals, respectively. More specifically, if we change the intrinsic pulsar period by only $\pm 10^{-9}\%$ the timing residuals exceed the sensitivity threshold after only two orbital periods (~ 3 months of observations). On the other hand, varying \dot{P} of order 0.1% makes the residuals exceed the sensitivity threshold after ~ 4.5 orbital periods (~ 7.5 months of observations). We point out that changing intrinsic parameters, such as the pulsar period P and its derivative \dot{P} , changes the shape and amplitude of the residuals but does not alter the orbit of the pulsar (nor the photon travel time). In fact, those changes in the shape and amplitude of the residuals do not depend on the particular system. For example, if we consider Toy 1 and Toy 3, the effect of varying P and \dot{P} will be the same, with the only difference being in the number of orbital periods required by their residuals to exceed the experimental detectability threshold.

Varying the mass M of the gravitational source, panel (c) of Figure 5, or of the orbital elements, panels (e) and (f) of Figure 5 for the semi-major axis a and eccentricity e , respectively, affects the orbital dynamic itself of the pulsar. Therefore, secular effects will appear, accumulate and grow in amplitude on each orbit, leaving a detectable imprint on the shape and amplitude of the residuals. This is especially true for the mass of the central object M and the semi-major axis of the pulsar orbits a , whose variations induce residuals with a linearly growing amplitude. When we vary the eccentricity e , on the other hand, the residuals show a constant amplitude at apocenter which scales proportionally to the semi-major axis (and does not increase over time), while the secular effect on the residuals only appears at apocenter (owing to the modified rate of orbital precession), whose amplitude exhibits a slower growth compared to the previous cases. Overall, this result clearly shows how the timing analysis of pulsars at the Galactic Center can not only provide incredibly tight constraints on the orbital elements of these objects, but also on the mass of the central SMBH which can reach, which, with only a few months of observations, can surpass by orders of magnitudes the current precision from S-stars orbits.

Finally, in panel (g) of Figure 5, we study the impact of changing the orbital inclination i on the residuals. In this case, the amplitude is fixed because misestimating the angular orbital parameters does not induce (at first

order) a secular variation of the orbits. One must misestimate the inclinations of a factor $\sim 10^{-6}\%$ to exceed the sensitivity threshold.

By repeating this analysis for all the toy models considered in Table I, we obtain an estimate of the number of complete orbits (and hence of the observation timespan) required for the timing residuals to exceed the nominal timing sensitivity for SKA-like observations of pulsars at the Galactic Center. We summarize all these results in Table II for the toy models reported in Table I. Specifically, for individual variations of one parameter at a time (by leaving all other parameters fixed) within given percentages, we report the number of periods and the corresponding time required for the residuals amplitude to surpass the threshold. The results are consistent across the four toy models considered, with pulsars in a stronger gravitational regime requiring a shorter observational window to qualitatively reach the same percentage sensitivity on the orbital parameters (with only the eccentricity, due to the aforementioned non-linear behaviour on the timing residuals, representing an exception to this pattern), while intrinsic parameters, like the pulsar period and its variation, whose estimation is independent on the strength of the gravitational regime, require the same amount of time across the different models.

B. Failure of weak field timing techniques

The procedures introduced in the previous sections to compute TOAs for pulsars around a SMBH described by the Schwarzschild spacetime, also allows for an interesting comparison between results of the fully relativistic procedure (described in Section III B) and the ones obtained using formulas that rely on the first-order post-Newtonian approximation, and are implemented in all current codes devoted to TOA analysis [43, 50, 55], described in Section III A. Specifically, for a given set of orbital and intrinsic parameters we compute a geodesic orbit for the pulsar covering one full orbital period, by numerical integration of Eqs. (6)-(9). We sample emission proper times over the considered period and, at those positions on the orbit, we apply our fully relativistic methodology to compute the corresponding TOA at the distant observer's location. At the same time, we consider a PN orbit as described in [40], upon considering an infinite mass ratio between the test particle and the companion. We then consider emission times corresponding to the same pulses in the pulse sequence as those used for the fully relativistic calculation, and, from the position of the pulsar at these instants of time, we compute PN TOAs, using Eq. (27). Since we are using harmonic coordinates for the geodesic integration, we can directly compare the two estimates of the propagation time, as the two are expressed in the same coordinate system. A useful way to assess the difference between the two methodologies is to consider the maximum amplitude, over the

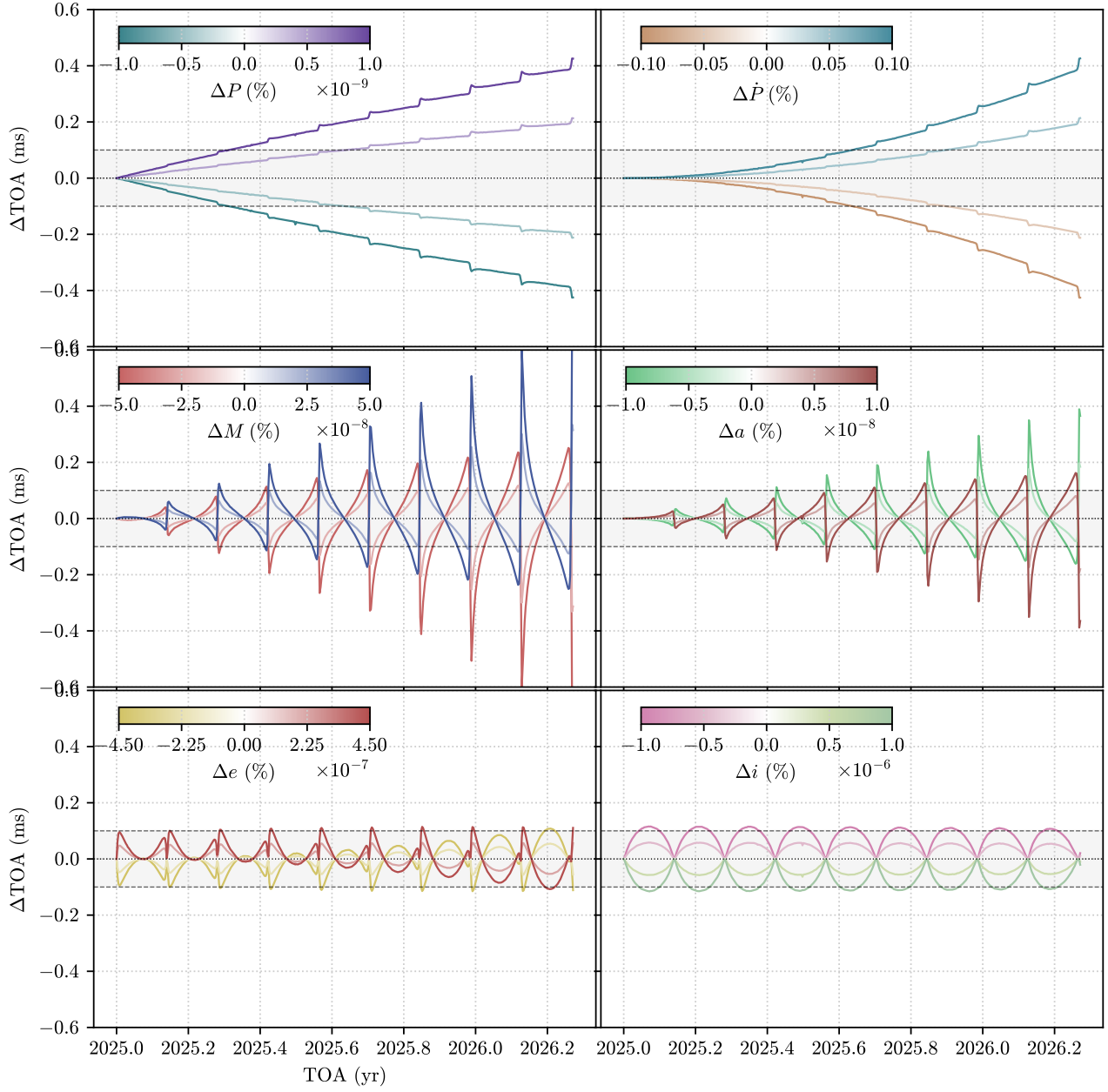


Figure 5. Timing residuals over 10 orbits for the Toy 2 model (see Table I), generated by slightly modifying each intrinsic or orbital parameter of the pulsar by the percentage indicated in the colorbar of each panel. Residuals are calculated by varying one parameter at a time while keeping all others fixed. The horizontal shaded regions represent the expected nominal timing accuracy for SKA observations in the Galactic Center, set at $100 \mu\text{s}$.

considered period, of the difference between the PN and the fully relativistic photon propagation time. Due to the way current timing codes compute the pulse phase, and thus the residuals, from the coordinate time of observation of any pulse (see Section III A), whenever the discrepancy that we are computing surpasses the pulsar intrinsic period, it implies the failure of the PN-based timing formulas to correctly identify the emission pulse within the pulse sequence, and thus, the failure of the

whole timing procedure in obtaining phase-connected residuals. The results of this analysis are shown in Figure ??, which illustrates the maximum discrepancy over one orbital period between the PN approximation and the fully relativistic approach for pulsar timing around a SMBH. The results consider the mass of Sgr A* and include two cases: circular orbits (left panel) and a highly eccentric S2-like orbit with $e = 0.88$ (right panel). For both cases, discrepancies are calculated across a range of

Parameter	Precision	Toy 0 (S2-like)		Toy 1		Toy 2		Toy 3	
		Orbits	Time	Orbits	Time	Orbits	Time	Orbits	Time
P	$5 \times 10^{-10}\%$	0.03	6 months	0.5	6 months	4	6 months	90	6 months
	$1 \times 10^{-9}\%$	0.015	3 months	0.25	3 months	2	3 months	45	3 months
\dot{P}	$5 \times 10^{-2}\%$	0.05	10 months	0.75	10 months	6	10 months	110	10 months
	$1 \times 10^{-1}\%$	0.04	7.5 months	0.55	7.5 months	4.5	7.5 months	60	7.5 months
M	$2.5 \times 10^{-8}\%$	0.73	11.6 years	2	2.5 years	3	5 months	17	1 month
	$5 \times 10^{-8}\%$	0.63	10 years	1	1 year	2	3.5 months	12	25 days
a	$5 \times 10^{-9}\%$	0.71	11.3 years	4	3.5 years	10	1.5 years	30	60 days
	$1 \times 10^{-8}\%$	0.5	8.2 years	3	2.5 years	3	5 months	16	32 days
e	$2.5 \times 10^{-7}\%$	1	16 years	1	1.2 years	20	2.4 years	11	19 days
	$5 \times 10^{-7}\%$	1	16 years	1	1.2 years	10	1.2 years	4	7 days
i	Case by case	0.5	8 years	0.5	6 months	0.5	25 days	0.5	1 day
		$(5 \times 10^{-8}\%)$		$(7 \times 10^{-7}\%)$		$(1 \times 10^{-6}\%)$		$(1 \times 10^{-5}\%)$	

Table II. The time (and corresponding number of complete orbits) required for the TOA residuals to surpass the nominal timing accuracy of $100 \mu\text{s}$, expected for SKA observations of pulsars in the Galactic Center. For each toy model analyzed, the table lists the time needed to achieve the precision (in percentage) indicated in the second column for each of the pulsar’s orbital and intrinsic parameters.

semi-major axes, $a \in [50, 30000]M$ (or $[2, 1300]$ AU for Sgr A*), and for three orbital inclinations. A key feature highlighted in the figure is the significant impact of orbital inclination on timing discrepancies, with edge-on orbits showing the largest deviations due to pronounced strong lensing effects. Even for an orbit with same semi-major axis and inclination as S2 the resulting discrepancy is of order 10^{-1} s, three orders of magnitude above the nominal SKA sensibility, and thus potentially able to spoil the ability to perform timing with current techniques. For smaller semi-major axes and more eccentric orbits, this effect is even more drastic, emphasizing the importance of fully relativistic modeling for precise timing near SMBHs and the failure of the PN approximation to appropriately account for the fully non linear effects of General Relativity.

V. DISCUSSIONS AND CONCLUSIONS

The detection and precise timing of pulsars orbiting a SMBH, such as Sgr A* at the Galactic Center, represent

an unparalleled opportunity to explore the strong-field regime of General Relativity and test alternative theories of gravity [33, 37]. Despite the challenges posed by interstellar scattering and observational limitations, the supposed existence of a substantial pulsar population near Sgr A* [23–27] strongly motivates continued efforts to detect and analyze these systems using advanced observational facilities like SKA [28], FAST [29], ngVLA [30], and ngEHT [31].

Our work builds upon this premise by introducing a novel approach to computing the photon propagation time in black hole spacetimes. This methodology, first introduced in [37], allows for more precise modeling of pulse TOAs at an Earth-based observatory and highlights the inadequacies of traditional post-Newtonian approximations in these extreme environments. By comparing our relativistic approach with standard techniques, we demonstrate that our framework provides significantly improved accuracy, paving the way for more reliable measurements of the SMBH’s mass (and possibly its spin and quadrupole moment), enabling robust tests of the black hole paradigm.

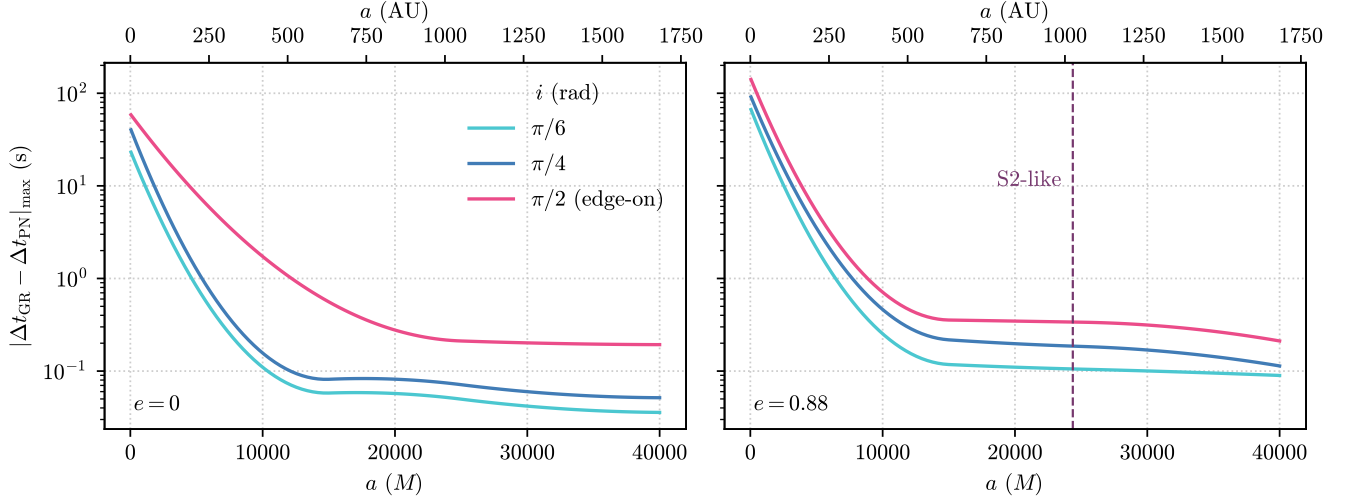


Figure 6. Maximum discrepancy over one orbital period between the post-Newtonian approximation and the fully relativistic methodology for pulsar timing around a SMBH. In particular, we are considering the mass of the central object to be that of Sgr A* and we consider two values of eccentricity corresponding to circular orbits (*left panel*) and to an S2-like orbit with $e = 0.88$ (*right panel*). For each of the considered eccentricities we compute the discrepancy between the two timing estimates for a range of semi-major axes spanning the interval $a \in [50, 30000]M$ (corresponding to $[2, 1300]$ AU for Sgr A*) and for three values of the inclination, as indicated in the legend (the pink line corresponds to the most extreme case of an edge-on orbit for which the discrepancy is always maximized due to the strong lensing effects in this case).

In Section II we summarized the numerical methodology, first introduced in [37] for the numerical computation of fully relativistic propagation times for photons emitted in a generic spherically symmetric spacetime, particularizing it for the Schwarzschild solution in harmonic coordinates, that are usually employed by timing codes based on the post-Newtonian approximation (of which we have given an overview in Section III A).

In Sections III B and IV A we have extended our methodology not only to compute the general relativistic photon propagation time but also to develop a timing model to generate phase-connected residuals and perform fitting of TOAs data to a Schwarzschild model. Considering several toy model pulsars, we showed how this methodology can be used to quantitatively estimate the phase-dependent residuals arising from a misestimation of one of the pulsar’s parameters. Such estimates, on the other hand, gave us a qualitative idea of the possible precision that would be achieved through an actual fitting analysis of our timing model on TOAs data. For example, we demonstrated a remarkable sensitivity of timing residuals to variations of the mass of central object as small as $\sim 10^{-8}\%$ of its value. This, even for an S2-like orbit, hints at the possibility of characterizing within only a few years of observations (or months, for more extreme orbital configurations) the gravitational field of the central SMBH of the Milky Way with a precision that is well beyond current estimates using orbital fitting of the S-Stars (current constrains on the mass of Sgr A* using these orbital data allow to determine its mass with a precision

of $\sim 0.2\%$). The same also applies to the other orbital and intrinsic pulsar parameters.

On the other hand, in Section IV B we have shown how the fully relativistic estimates of the TOAs at a distant observer significantly differ from their corresponding estimates using both pulsar trajectories and photon propagation times computed with the same post-Newtonian formulas used in popular pulsar timing codes [40, 43, 50]. This result, strongly favours the application of a fully relativistic methodology to compute TOAs in the strong field regime of a SMBH, highlighting the failure of the first-order post-Newtonian approximation in fully capturing the non-linear effects of the geodesic motion for both the pulsar and the photons emitted by it. Arguably, these issues might be alleviated extending current timing codes to include higher-order terms in the post-Newtonian expansion. However, this quickly becomes impractical whenever one wants to test black hole models in theoretical frameworks beyond General Relativity. Our methodology, on the other hand, is fully general and can be applied to any spherically symmetric space-time, providing fully-relativistic TOAs within any given numerical precision.

Our work-in-progress study highlights the great constraining power enabled by pulsar timing observations and the importance of properly accounting for all relativistic effects by adopting a geodesic timing model. The next major step to implement, in order to provide a more realistic description of the central object, is to extend the methodology that we have developed to a rotating black

hole solution, like the Kerr black hole in General Relativity or its mimickers and extensions in modified theories of gravity.

ACKNOWLEDGEMENTS

IDM and RDM acknowledge support from the grant PID2021-122938NB-I00 funded by

MCIN/AEI/10.13039/501100011033 and by “ERDF A way of making Europe”. RDM also acknowledges support from Consejería de Educación de la Junta de Castilla y León and the European Social Fund. IDM also acknowledges support from the grant SA097P24 funded by Junta de Castilla y León and by “ERDF A way of making Europe”.

-
- [1] W. Becker, M. Kramer, and A. Sesana, *Space Sci. Rev.* **214**, 30 (2018), arXiv:1705.11022 [astro-ph.IM].
- [2] I. H. Stairs, *Living Reviews in Relativity* **6**, 5 (2003), arXiv:astro-ph/0307536 [astro-ph].
- [3] D. R. Lorimer, *Living Reviews in Relativity* **11**, 8 (2008), arXiv:0811.0762 [astro-ph].
- [4] C. M. Will, *Living Reviews in Relativity* **17**, 4 (2014), arXiv:1403.7377 [gr-qc].
- [5] R. A. Hulse and J. H. Taylor, *ApJ* **195**, L51 (1975).
- [6] J. Taylor, Joseph H., *Reviews of Modern Physics* **66**, 711 (1994).
- [7] M. Kramer, I. H. Stairs, R. N. Manchester, M. A. McLaughlin, A. G. Lyne, R. D. Ferdman, M. Burgay, D. R. Lorimer, A. Possenti, N. D’Amico, J. M. Sarkissian, G. B. Hobbs, J. E. Reynolds, P. C. C. Freire, and F. Camilo, *Science* **314**, 97 (2006), arXiv:astro-ph/0609417 [astro-ph].
- [8] F. Zhang and P. Saha, *ApJ* **849**, 33 (2017), arXiv:1709.08341.
- [9] S. Johnston, M. A. Walker, M. H. van Kerkwijk, A. G. Lyne, and N. D’Amico, *MNRAS* **274**, L43 (1995).
- [10] S. Johnston, M. Kramer, D. R. Lorimer, A. G. Lyne, M. McLaughlin, B. Klein, and R. N. Manchester, *MNRAS* **373**, L6 (2006), arXiv:astro-ph/0606465 [astro-ph].
- [11] J. S. Deneva, J. M. Cordes, and T. J. W. Lazio, *ApJ* **702**, L177 (2009), arXiv:0908.1331 [astro-ph.SR].
- [12] J. S. Deneva, *Elusive neutron star populations: Galactic center and intermittent pulsars*, Ph.D. thesis, Cornell University, New York (2010).
- [13] S. D. Bates, S. Johnston, D. R. Lorimer, M. Kramer, A. Possenti, M. Burgay, B. Stappers, M. J. Keith, A. Lyne, M. Bailes, M. A. McLaughlin, J. T. O’Brien, and G. Hobbs, *MNRAS* **411**, 1575 (2011), arXiv:1009.5873 [astro-ph.SR].
- [14] J. A. Kennea, D. N. Burrows, C. Kouveliotou, D. M. Palmer, E. Göğüş, Y. Kaneko, P. A. Evans, N. Degenaar, M. T. Reynolds, J. M. Miller, R. Wijnands, K. Mori, and N. Gehrels, *ApJ* **770**, L24 (2013), arXiv:1305.2128 [astro-ph.HE].
- [15] K. Mori, E. V. Gotthelf, S. Zhang, H. An, F. K. Baganoff, N. M. Barrière, A. M. Beloborodov, S. E. Boggs, F. E. Christensen, W. W. Craig, F. Dufour, B. W. Grefenstette, C. J. Hailey, F. A. Harrison, J. Hong, V. M. Kaspi, J. A. Kennea, K. K. Madsen, C. B. Markwardt, M. Nynka, D. Stern, J. A. Tomsick, and W. W. Zhang, *ApJ* **770**, L23 (2013), arXiv:1305.1945 [astro-ph.HE].
- [16] N. Rea, P. Esposito, J. A. Pons, R. Turolla, D. F. Torres, G. L. Israel, A. Possenti, M. Burgay, D. Viganò, A. Papitto, R. Perna, L. Stella, G. Ponti, F. K. Baganoff, D. Haggard, A. Camero-Arranz, S. Zane, A. Minter, S. Mereghetti, A. Tiengo, R. Schödel, M. Feroci, R. Mignani, and D. Götz, *ApJ* **775**, L34 (2013), arXiv:1307.6331 [astro-ph.GA].
- [17] M. E. Lower, S. Dai, and S. Johnston, arXiv e-prints, arXiv:2404.09098 (2024), arXiv:2404.09098 [astro-ph.HE].
- [18] J. M. Cordes and T. J. W. Lazio, arXiv e-prints, astro-ph/0207156 (2002), arXiv:astro-ph/0207156 [astro-ph].
- [19] R. P. Eatough, M. Kramer, B. Klein, R. Karuppusamy, D. J. Champion, P. C. C. Freire, N. Wex, and K. Liu, *IAU Symp.* **291**, 382 (2013), arXiv:1210.3770 [astro-ph.GA].
- [20] R. S. Wharton, S. Chatterjee, J. M. Cordes, J. S. Deneva, and T. J. W. Lazio, *ApJ* **753**, 108 (2012), arXiv:1111.4216 [astro-ph.HE].
- [21] P. Torne, G. Desvignes, R. P. Eatough, M. Kramer, R. Karuppusamy, K. Liu, A. Noutsos, R. Wharton, C. Kramer, S. Navarro, G. Paubert, S. Sanchez, M. Sanchez-Portal, K. F. Schuster, H. Falcke, and L. Rezzolla, *A&A* **650**, A95 (2021), arXiv:2103.16581 [astro-ph.HE].
- [22] P. Torne, K. Liu, R. P. Eatough, J. Wongpcheausorn, J. M. Cordes, G. Desvignes, M. De Laurentis, M. Kramer, S. M. Ransom, S. Chatterjee, R. Wharton, R. Karuppusamy, L. Blackburn, M. Janssen, C.-k. Chan, B. Crew, Geoffrey, L. D. Matthews, C. Goddi, H. Rottmann, J. Wagner, S. Sánchez, I. Ruiz, F. Abbate, G. C. Bower, J. J. Salamanca, A. I. Gómez-Ruiz, A. Herrera-Aguilar, W. Jiang, R.-S. Lu, U.-L. Pen, A. W. Raymond, L. Shao, Z. Shen, G. Paubert, M. Sanchez-Portal, C. Kramer, M. Castillo, S. Navarro, D. John, K.-F. Schuster, M. D. Johnson, K. L. J. Rygl, K. Akiyama, A. Alberdi, W. Alef, J. C. Algaba, R. Anantua, K. Asada, R. Azulay, U. Bach, A.-K. Baczko, D. Ball, M. Baloković, J. Barrett, M. Bauböck, B. A. Benson, D. Bintley, R. Blundell, K. L. Bouman, H. Boyce, M. Bremer, C. D. Brinkerink, R. Brissenden, S. Britzen, A. E. Broderick, D. Brogiere, T. Bronzwaer, S. Bustamante, D.-Y. Byun, J. E. Carlstrom, C. Ceccobello, A. Chael, D. O. Chang, K. Chatterjee, M.-T. Chen, Y. Chen, X. Cheng, I. Cho, P. Christian, N. S. Conroy, J. E. Conway, T. M. Crawford, A. Cruz-Orsio, Y. Cui, R. Dahale, J. Davelaar, R. Deane, J. Dempsey, J. Dexter, V. Dhruv, S. S. Doeleman, S. Dougal, S. A. Dzib, R. Emami, H. Falcke, J. Farah, V. L. Fish, E. Fomalont, H. A. Ford, M. Foschi, R. Fraga-Encinas, W. T. Freeman, P. Friberg, C. M. Fromm, A. Fuentes, P. Galison, C. F. Gammie, R. García, O. Gentaz, B. Georgiev, R. Gold, J. L. Gómez, M. Gu, M. Gurwell, K. Hada, D. Hag-

- gard, K. Haworth, M. H. Hecht, R. Hesper, D. Heumann, L. C. Ho, P. Ho, M. Honma, C.-W. L. Huang, L. Huang, D. H. Hughes, S. Ikeda, C. M. V. Impellizzeri, M. Inoue, S. Issaoun, D. J. James, B. T. Jannuzi, B. Jeter, A. Jiménez-Rosales, S. Jorstad, A. V. Joshi, T. Jung, M. Karami, T. Kawashima, G. K. Keating, M. Kettenis, D.-J. Kim, J.-Y. Kim, J. Kim, J. Kim, M. Kino, J. Y. Koay, P. Kocherlakota, Y. Kofuji, S. Koyama, T. P. Krichbaum, C.-Y. Kuo, N. La Bella, T. R. Lauer, D. Lee, S.-S. Lee, P. K. Leung, A. Levis, Z. Li, R. Lico, G. Lindahl, M. Lindqvist, M. Lisakov, J. Liu, E. Liuzzo, W.-P. Lo, A. P. Lobanov, L. Loinard, C. J. Lonsdale, N. R. MacDonald, J. Mao, N. Marchili, S. Markoff, D. P. Marrone, A. P. Marscher, I. Martí-Vidal, S. Matsushita, L. Medeiros, K. M. Menten, D. Michalik, I. Mizuno, Y. Mizuno, J. M. Moran, K. Moriyama, M. Moscibrodzka, C. Müller, H. Müller, A. Mus, G. Musoke, I. Myserlis, A. Nadolski, H. Nagai, N. M. Nagar, M. Nakamura, R. Narayan, G. Narayanan, I. Natarajan, A. Nathanail, J. Neilsen, R. Neri, C. Ni, A. Noutsos, M. A. Nowak, J. Oh, H. Okino, H. Olivares, G. N. Ortiz-León, T. Oyama, F. Özel, D. C. M. Palumbo, G. F. Paraschos, J. Park, H. Parsons, N. Patel, D. W. Pesce, V. Piétu, R. Plambeck, A. PopStefanija, O. Porth, F. M. Pözl, B. Prather, J. A. Preciado-López, D. Psaltis, H.-Y. Pu, V. Ramakrishnan, R. Rao, M. G. Rawlings, L. Rezzolla, A. Ricarte, B. Ripperda, F. Roelofs, A. Rogers, E. Ros, C. Romero-Cañizales, A. Roshanineshat, A. L. Roy, C. Ruzsarczyk, D. Sánchez-Argüelles, M. Sasada, K. Satapathy, T. Savolainen, F. P. Schloerb, J. Schonfeld, D. Small, B. W. Sohn, J. SooHoo, K. Souccar, H. Sun, A. J. Tetarenko, P. Tiede, R. P. J. Tilanus, M. Titus, T. Toscano, E. Traianou, T. Trent, S. Trippe, M. Turk, I. van Bemmell, H. J. van Langevelde, D. R. van Rossum, J. Vos, D. Ward-Thompson, J. Wardle, J. Weintroub, N. Wex, M. Wielgus, K. Wiik, G. Witzel, M. F. Wondrak, G. N. Wong, Q. Wu, N. Yadlapalli, P. Yamaguchi, A. Yfantis, D. Yoon, A. Young, K. Young, Z. Younsi, W. Yu, F. Yuan, Y.-F. Yuan, J. A. Zensus, S. Zhang, G.-Y. Zhao, and S.-S. Zhao, *ApJ* **959**, 14 (2023), arXiv:2308.15381 [astro-ph.HE].
- [23] D. F. Figer, in *Massive Stars: From Pop III and GRBs to the Milky Way. Space Telescope Science Institute Symposium Series No. 20. Edited by Mario Livio and Eva Villaver. Cambridge University Press*, edited by M. Livio and E. Villaver (2009) pp. 40–59.
- [24] E. Pfahl and A. Loeb, *ApJ* **615**, 253 (2004), arXiv:astro-ph/0309744 [astro-ph].
- [25] F. Zhang, Y. Lu, and Q. Yu, *ApJ* **784**, 106 (2014), arXiv:1402.2505 [astro-ph.GA].
- [26] K. M. Rajwade, D. R. Lorimer, and L. D. Anderson, *MNRAS* **471**, 730 (2017), arXiv:1611.06977 [astro-ph.HE].
- [27] J. Chennamangalam and D. R. Lorimer, *MNRAS* **440**, L86 (2014), arXiv:1311.4846 [astro-ph.HE].
- [28] E. Keane, B. Bhattacharyya, M. Kramer, B. Stappers, E. F. Keane, B. Bhattacharyya, M. Kramer, B. W. Stappers, S. D. Bates, M. Burgay, S. Chatterjee, D. J. Champion, R. P. Eatough, J. W. T. Hessels, G. Janssen, K. J. Lee, J. van Leeuwen, J. Margueron, M. Oertel, A. Possenti, S. Ransom, G. Theureau, and P. Torne, in *Advancing Astrophysics with the Square Kilometre Array (AASKA14)* (2015) p. 40, arXiv:1501.00056 [astro-ph.IM].
- [29] R. Nan, D. Li, C. Jin, Q. Wang, L. Zhu, W. Zhu, H. Zhang, Y. Yue, and L. Qian, *International Journal of Modern Physics D* **20**, 989 (2011), arXiv:1105.3794 [astro-ph.IM].
- [30] G. C. Bower, A. Broderick, J. Dexter, S. Doeleman, H. Falcke, V. Fish, M. D. Johnson, D. P. Marrone, J. M. Moran, M. Moscibrodzka, A. Peck, R. L. Plambeck, and R. Rao, *ApJ* **868**, 101 (2018), arXiv:1810.07317 [astro-ph.HE].
- [31] K. Akiyama, A. Alberdi, W. Alef, J. C. Algaba, R. Anantua, K. Asada, R. Azulay, U. Bach, A.-K. Baczko, D. Ball, and et al., *ApJ* **930**, L12 (2022).
- [32] N. Wex and S. M. Kopeikin, *ApJ* **514**, 388 (1999), arXiv:astro-ph/9811052 [astro-ph].
- [33] K. Liu, N. Wex, M. Kramer, J. M. Cordes, and T. J. W. Lazio, *ApJ* **747**, 1 (2012), arXiv:1112.2151 [astro-ph.HE].
- [34] D. Psaltis, N. Wex, and M. Kramer, *ApJ* **818**, 121 (2016), arXiv:1510.00394 [astro-ph.HE].
- [35] P. Christian, D. Psaltis, and A. Loeb, arXiv e-prints, arXiv:1511.01901 (2015), arXiv:1511.01901 [gr-qc].
- [36] R. N. Izmailov, E. R. Zhdanov, A. Bhadra, and K. K. Nandi, *European Physical Journal C* **79**, 105 (2019).
- [37] R. Della Monica, I. De Martino, and M. De Laurentis, *MNRAS* **524**, 3782 (2023), arXiv:2305.18178 [gr-qc].
- [38] M. De Laurentis, I. de Martino, and R. Della Monica, *Reports on Progress in Physics* **86**, 104901 (2023), arXiv:2211.07008 [astro-ph.GA].
- [39] R. Eatough, T. J. W. Lazio, J. Casanellas, S. Chatterjee, J. M. Cordes, P. B. Demorest, M. Kramer, K. J. Lee, K. Liu, S. M. Ransom, and N. Wex, in *Advancing Astrophysics with the Square Kilometre Array (AASKA14)* (2015) p. 45, arXiv:1501.00281 [astro-ph.IM].
- [40] T. Damour and N. Deruelle, *Ann. Inst. Henri Poincaré Phys. Théor* **44**, 263 (1986).
- [41] E. Hackmann and A. Dhani, *General Relativity and Gravitation* **51**, 37 (2019), arXiv:1806.02547 [gr-qc].
- [42] F. W. J. Olver, A. B. O. Daalhuis, D. W. Lozier, B. I. Schneider, R. F. Boisvert, C. W. Clark, B. V. S. B. R. Mille and, H. S. Cohl, and e. M. A. McClain, “Nist digital library of mathematical functions,” <http://dlmf.nist.gov/>, Release 1.0.26 of 2020-03-15 (2020).
- [43] R. T. Edwards, G. B. Hobbs, and R. N. Manchester, *MNRAS* **372**, 1549 (2006), arXiv:astro-ph/0607664 [astro-ph].
- [44] D. Lai and R. R. Rafikov, *ApJ* **621**, L41 (2005), arXiv:astro-ph/0411726 [astro-ph].
- [45] J. H. Taylor, L. A. Fowler, and P. M. McCulloch, *Nature* **277**, 437 (1979).
- [46] J. H. Taylor and J. M. Weisberg, *ApJ* **345**, 434 (1989).
- [47] A. Wolszczan and D. A. Frail, *Nature* **355**, 145 (1992).
- [48] V. M. Kaspi, J. H. Taylor, and M. F. Ryba, *ApJ* **428**, 713 (1994).
- [49] R. T. Edwards, W. van Straten, and M. Bailes, *ApJ* **560**, 365 (2001), arXiv:astro-ph/0106353 [astro-ph].
- [50] G. B. Hobbs, R. T. Edwards, and R. N. Manchester, *MNRAS* **369**, 655 (2006), arXiv:astro-ph/0603381 [astro-ph].
- [51] G. Agazie, A. Anumarlapudi, A. M. Archibald, Z. Arzoumanian, P. T. Baker, B. Bécsy, L. Blecha, A. Brazier, P. R. Brook, S. Burke-Spolaor, R. Burnette, R. Case, M. Charisi, S. Chatterjee, K. Chatziioannou, B. D. Cheeseboro, S. Chen, T. Cohen, J. M. Cordes, N. J.

- Cornish, F. Crawford, H. T. Cromartie, K. Crowter, C. J. Cutler, M. E. Deesar, D. Degan, P. B. Demorest, H. Deng, T. Dolch, B. Drachler, J. A. Ellis, E. C. Ferrara, W. Fiore, E. Fonseca, G. E. Freedman, N. Garver-Daniels, P. A. Gentile, K. A. Gersbach, J. Glaser, D. C. Good, K. Gültekin, J. S. Hazboun, S. Hourihane, K. Islo, R. J. Jennings, A. D. Johnson, M. L. Jones, A. R. Kaiser, D. L. Kaplan, L. Z. Kelley, M. Kerr, J. S. Key, T. C. Klein, N. Laal, M. T. Lam, W. G. Lamb, T. J. W. Lazio, N. Lewandowska, T. B. Littenberg, T. Liu, A. Lommen, D. R. Lorimer, J. Luo, R. S. Lynch, C.-P. Ma, D. R. Madison, M. A. Mattson, A. McEwen, J. W. McKee, M. A. McLaughlin, N. McMann, B. W. Meyers, P. M. Meyers, C. M. F. Mingarelli, A. Mitridate, P. Nataraajan, C. Ng, D. J. Nice, S. K. Ocker, K. D. Olum, T. T. Pennucci, B. B. P. Perera, P. Petrov, N. S. Pol, H. A. Radovan, S. M. Ransom, P. S. Ray, J. D. Romano, S. C. Sardesai, A. Schmiedekamp, C. Schmiedekamp, K. Schmitz, L. Schult, B. J. Shapiro-Albert, X. Siemens, J. Simon, M. S. Siwek, I. H. Stairs, D. R. Stinebring, K. Stovall, J. P. Sun, A. Susobhanan, J. K. Swiggum, J. Taylor, S. R. Taylor, J. E. Turner, C. Unal, M. Vallisneri, R. van Haasteren, S. J. Vigeland, H. M. Wahl, Q. Wang, C. A. Witt, O. Young, and Nanograv Collaboration, *ApJ* **951**, L8 (2023), arXiv:2306.16213 [astro-ph.HE].
- [52] EPTA Collaboration, InPTA Collaboration, J. Antoniadis, P. Arumugam, S. Arumugam, S. Babak, M. Bagchi, A. S. Bak Nielsen, C. G. Bassa, A. Bathula, A. Berthreau, M. Bonetti, E. Bortolas, P. R. Brook, M. Burgay, R. N. Caballero, A. Chalumeau, D. J. Champion, S. Chanlaridis, S. Chen, I. Cognard, S. Dandapat, D. Deb, S. Desai, G. Desvignes, N. Dhanda-Batra, C. Dwivedi, M. Falxa, R. D. Ferdman, A. Franchini, J. R. Gair, B. Goncharov, A. Gopakumar, E. Graikou, J. M. Grießmeier, L. Guillemot, Y. J. Guo, Y. Gupta, S. Hisano, H. Hu, F. Iraci, D. Izquierdo-Villalba, J. Jang, J. Javor, G. H. Janssen, A. Jessner, B. C. Joshi, F. Kareem, R. Karuppusamy, E. F. Keane, M. J. Keith, D. Kharbanda, T. Kikunaga, N. Kolhe, M. Kramer, M. A. Krishnakumar, K. Lackeos, K. J. Lee, K. Liu, Y. Liu, A. G. Lyne, J. W. McKee, Y. Maan, R. A. Main, M. B. Mickaliger, I. C. Nițu, K. Nobleson, A. K. Paladi, A. Parthasarathy, B. B. P. Perera, D. Perrodin, A. Petiteau, N. K. Porayko, A. Possenti, T. Prabu, H. Quelquejay Leclere, P. Rana, A. Samajdar, S. A. Sanidas, A. Sesana, G. Shaifullah, J. Singha, L. Speri, R. Spiewak, A. Srivastava, B. W. Stappers, M. Surnis, S. C. Susarla, A. Susobhanan, K. Takahashi, P. Tarafdar, G. Theureau, C. Tiburzi, E. van der Wateren, A. Vecchio, V. Venkatraman Krishnan, J. P. W. Verbiest, J. Wang, L. Wang, and Z. Wu, *A&A* **678**, A50 (2023), arXiv:2306.16214 [astro-ph.HE].
- [53] D. J. Reardon, A. Zic, R. M. Shannon, G. B. Hobbs, M. Bailes, V. Di Marco, A. Kapur, A. F. Rogers, E. Thrane, J. Askew, N. D. R. Bhat, A. Cameron, M. Curylo, W. A. Coles, S. Dai, B. Goncharov, M. Kerr, A. Kulkarni, Y. Levin, M. E. Lower, R. N. Manchester, R. Mandow, M. T. Miles, R. S. Nathan, S. Osłowski, C. J. Russell, R. Spiewak, S. Zhang, and X.-J. Zhu, *ApJ* **951**, L6 (2023), arXiv:2306.16215 [astro-ph.HE].
- [54] H. Xu, S. Chen, Y. Guo, J. Jiang, B. Wang, J. Xu, Z. Xue, R. Nicolas Caballero, J. Yuan, Y. Xu, J. Wang, L. Hao, J. Luo, K. Lee, J. Han, P. Jiang, Z. Shen, M. Wang, N. Wang, R. Xu, X. Wu, R. Manchester, L. Qian, X. Guan, M. Huang, C. Sun, and Y. Zhu, *Research in Astronomy and Astrophysics* **23**, 075024 (2023), arXiv:2306.16216 [astro-ph.HE].
- [55] J. Luo, S. Ransom, P. Demorest, P. S. Ray, A. Archibald, M. Kerr, R. J. Jennings, M. Bachetti, R. van Haasteren, C. A. Champagne, J. Colen, C. Phillips, J. Zimmerman, K. Stovall, M. T. Lam, and F. A. Jenet, *ApJ* **911**, 45 (2021), arXiv:2012.00074 [astro-ph.IM].
- [56] R. Blandford and S. A. Teukolsky, *ApJ* **205**, 580 (1976).
- [57] S. M. Kopeikin, *ApJ* **439**, L5 (1995).
- [58] S. M. Kopeikin, *ApJ* **467**, L93 (1996).
- [59] N. Wex, *MNRAS* **298**, 67 (1998), arXiv:astro-ph/9706086 [astro-ph].
- [60] D. R. Lorimer and M. Kramer, *Handbook of Pulsar Astronomy*, Vol. 4 (2004).